

# Evaluating $\text{Zn}_2\text{SiO}_4\text{:Mn}$ phosphor for use in medical imaging radiation detectors

I. Kandarakis<sup>1</sup>, D. Cavouras<sup>1</sup>, P. Prassopoulos<sup>2</sup>, E. Kanellopoulos<sup>1</sup>, C.D. Nomicos<sup>3</sup>, G.S. Panayiotakis<sup>4</sup>

<sup>1</sup>Dept. of Medical Instrumentation Technology, Technological Educational Institution of Athens, Ag. Spyridonos Street, Aigaleo, 122 10 Athens, Greece (Fax: +3-01/5910-975, E-mail: cavouras@hol.gr; cavouras@medisp.teiath.gr)

<sup>2</sup>Department of Radiology, University Hospital, Medical School, University of Crete, Heraklion, Greece

<sup>3</sup>Dept. of Electronics, Technological Educational Institution of Athens, Ag. Spyridonos Street, Aigaleo, 122 10 Athens, Greece

<sup>4</sup>Dept. of Medical Physics, Medical School, University of Patras, 265 00 Patras, Greece

Received: 31 July 1998/Accepted: 3 August 1998

**Abstract.**  $\text{Zn}_2\text{SiO}_4\text{:Mn}$  phosphor was evaluated for use in radiation detectors of medical imaging systems.  $\text{Zn}_2\text{SiO}_4\text{:Mn}$  was used in the form of laboratory-prepared fluorescent layers (screens) with coating weights from 18 to 150 mg/cm<sup>2</sup>. The phosphor was excited to luminescence by low-energy X-rays using X-ray tube voltages ranging from 15 to 50 kVp. The number of emitted optical photons per incident X-ray quantum was thus determined for various X-ray energies and phosphor coating weights. The optical emission spectrum was also measured and it was used to evaluate the spectral compatibility of  $\text{Zn}_2\text{SiO}_4\text{:Mn}$  with radiographic films, photocathodes and the Si photodiode. Finally, phosphor optical properties were estimated by fitting a theoretical model to experimental data. Results showed that  $\text{Zn}_2\text{SiO}_4\text{:Mn}$  is more efficient for low-energy X-rays. Its intrinsic conversion efficiency was found equal to 0.08, which is comparable to that of actually used phosphors.  $\text{Zn}_2\text{SiO}_4\text{:Mn}$  was also adequately compatible with orthochromatic films and the ES-20 photocathode, thus being appropriate for low-voltage radiography and fluoroscopy.

**PACS:** 78.65; 42.80

Phosphor materials are used as X-ray to light converters coupled to optical detectors in most X-ray or nuclear medicine imaging systems.  $\text{Zn}_2\text{SiO}_4\text{:Mn}$  is a phosphor that is used in non-medical applications [1], but, to our knowledge, it has never been employed in medical imaging. Previous studies on  $\text{Zn}_2\text{SiO}_4\text{:Mn}$  [2] have reported an intrinsic conversion efficiency under electron beam excitation of the order of 8%. This value is close to values of other phosphors employed in medical imaging [3], which, however, have been determined under X-ray excitation. Additionally, the light emitted by  $\text{Zn}_2\text{SiO}_4\text{:Mn}$  seems to be compatible with the spectral sensitivity of optical detectors (films, photocathodes, photodiodes) used in X-ray or nuclear imaging.

In this paper an evaluation of  $\text{Zn}_2\text{SiO}_4\text{:Mn}$  under X-ray excitation is presented in order to investigate the suitability of this material for medical image receptors. For this purpose, the following parameters were studied.

- (i) The number of emitted light photons (NEP) per incident X-ray quantum as a function of X-ray energy and phosphor coating weight.
- (ii) The emission spectrum and its compatibility with the spectral sensitivity of various optical detectors.
- (iii) The effective NEP, which expresses the spectrally useful fraction of emitted light.
- (iv) The optical properties (absorption, scattering, reflectivity) of  $\text{Zn}_2\text{SiO}_4\text{:Mn}$ .

## 1 Materials and methods

### 1.1 Theory and definitions

The light energy flux  $\Psi_\lambda$  emitted by a phosphor material excited by X-rays may be expressed as follows:

$$\Psi_\lambda(E_0, w) = \int_0^{E_0} \Psi_X(E) \eta_Q(E, w) \eta_C g_\lambda(E, E_\lambda, w) dE, \quad (1)$$

where,  $E_0$  is the maximum energy of the energy spectrum of the polyenergetic X-ray beam used to excite the phosphor,  $w$  is the coating weight of the phosphor layer,  $\Psi_X$  is the incident X-ray energy flux,  $E$  denotes the energy of an X-ray quantum,  $\eta_Q$  is the quantum detection efficiency expressing the fraction of incident X-ray quanta that are absorbed by the phosphor,  $\eta_C$  is the intrinsic X-ray to light conversion efficiency, which is the fraction of absorbed X-ray energy flux that is converted into light within the phosphor's mass,  $g_\lambda$  is the light transmission efficiency expressing the fraction of light that is transmitted through the phosphor layer and is emitted by the phosphor's surface, and  $E_\lambda$  is the energy of an optical quantum.

The number ( $n_\lambda$ ) of emitted optical quanta per incident X-ray, may be obtained by dividing relation (1) by: 1. The mean energy of an optical quantum  $E_\lambda$  so as to obtain the total number of emitted photons. 2. The incident X-ray quantum flux (X-ray quanta per unit of area and time); this flux may

be obtained by measuring the incident exposure rate  $\dot{X}$  and multiplying it by the exposure to X-ray quantum flux ( $\Phi_X$ ) conversion factor  $[\Phi_X/\dot{X}]$  [4, 5]. Thus, NEP is written as

$$n_\lambda(E_0, w) = \frac{1}{\bar{E}_\lambda \dot{X}} \int_0^{E_0} \frac{\Psi_X(E)}{[\Phi_X/\dot{X}]} \eta_Q(E, w) \eta_{CG\lambda}(E, E_\lambda, w) dE, \quad (2)$$

where

$$[\Phi_X/\dot{X}] = \frac{W_{\text{air}}}{[\mu_{\text{en}}/\rho]_{\text{air}} e E}. \quad (3)$$

$W_{\text{air}}$  is the average energy required to produce an ion pair in air,  $[\mu_{\text{en}}/\rho]_{\text{air}}$  is the mass X-ray energy absorption coefficient of air and  $e$  is the electron charge [4, 5].

The mean energy  $\bar{E}_\lambda$  of the emitted optical photons may be determined by averaging  $E_\lambda$  over the phosphor's emission spectrum ( $\varepsilon_p$ ) as follows:

$$\bar{E}_\lambda = \int_{\lambda_1}^{\lambda_2} \varepsilon_p(E_\lambda) E_\lambda dE_\lambda / \int_{\lambda_1}^{\lambda_2} \varepsilon_p(E_\lambda) dE_\lambda. \quad (4)$$

The spectral compatibility of the phosphor's emission spectrum  $\varepsilon_p(\lambda)$  with the spectral sensitivity  $S_{\text{OD}}(\lambda)$  of the optical detector coupled to the phosphor in medical image receptors, is assessed by the spectral matching factor  $a_S$  [6]. This factor may be determined by the formula

$$a_S = \int_{\lambda_1}^{\lambda_2} \varepsilon_p(\lambda) S_{\text{OD}}(\lambda) d\lambda / \int_{\lambda_1}^{\lambda_2} S_{\text{OD}}(\lambda) d\lambda, \quad (5)$$

where  $\lambda_1$  and  $\lambda_2$  are the lower and upper limiting wavelength values of  $\varepsilon_p(\lambda)$ .  $a_S$  gives the fraction of the emitted light energy flux that can sensitize the optical detector with respect to the detector's spectral sensitivity. Using relations (2) and (5), the effective number of emitted optical photons  $n_{\lambda, \text{eff}}$  may be defined as

$$n_{\lambda, \text{eff}}(E_0, w) = \frac{a_S}{\bar{E}_\lambda \dot{X}} \int_0^{E_0} \frac{\Psi_X(E)}{[\Phi_X/\dot{X}]} \eta_Q(E, w) \times \eta_{CG\lambda}(E, E_\lambda, w) dE. \quad (6)$$

$n_{\lambda, \text{eff}}$  gives the number of emitted photons per incident X-ray quantum that are useful for a specific phosphor–optical detector combination.

### 1.2 Experimental method

The  $\text{Zn}_2\text{SiO}_4\text{:Mn}$  phosphor was supplied in powder form (Derby Luminescents, Ltd.) with mean grain size of approximately 7  $\mu\text{m}$ . Phosphor layers (screens) with coating weights 18, 34, 56, 89, 115, and 153  $\text{mg}/\text{cm}^2$  were prepared by sedimentation as described in previous studies [7–10]. Screens were irradiated by low-energy X-rays with tube voltages ranging from 15 kVp to 50 kVp. At higher voltages the performance of  $\text{Zn}_2\text{SiO}_4\text{:Mn}$  is not satisfactory due to its low

effective atomic number. The emitted light energy flux  $\Psi_\lambda$  was measured by an EMI 9558 QB photomultiplier coupled to a Cary 401 electrometer. Measurements were performed following two modes of observation: 1. Front screen configuration setup (or transmission mode), where the light emitted from the non-irradiated phosphor surface was measured and 2. Back-screen configuration setup (or reflection mode), where the light emitted from the irradiated screen surface was determined. The first setup simulates the front screen of double-coated medical radiographic cassettes and all other types of medical imaging detectors, while the second setup simulates the back screen of double-coated radiographic cassettes and of the single-coated mammographic cassettes. Details of the measurement techniques are described in previous studies [7–9]. The exposure rate  $\dot{X}$  was measured using a PTW dosimeter (ionization chamber type No. 23333).

The emission spectrum  $\varepsilon_p(\lambda)$  of  $\text{Zn}_2\text{SiO}_4\text{:Mn}$  and the energy  $\bar{E}_\lambda = hc/\bar{\lambda}$  of the emitted optical quanta were determined by means of an Oriel 7240 grating monochromator.

### 1.3 Estimation of optical properties

Relation (2) was used to estimate the coefficients of optical photon absorption  $\mu_a$  and optical photon scattering  $\mu_s$ . This was accomplished by fitting relation (2) to experimental NEP data using the following functions and parameters.

The quantum detection efficiency  $\eta_Q$  was approximated by the formula

$$\eta_Q(E, w) = 1 - e^{-\mu(E)w}, \quad (7)$$

where  $\mu(E)$  is the X-ray absorption coefficient of the phosphor.  $\mu(E)$  was calculated using data on Zn, Si, and O from Storm and Israel [11].

The light transmission efficiency  $g_\lambda$  was expressed as follows:

$$g_\lambda(E, E_\lambda, w) = \int_0^{w_0} \Psi_R(E, w) g_w(\sigma, \beta, \rho, w) dw, \quad (8)$$

where  $\Psi_R$  is a function giving the relative X-ray energy flux absorbed at the elementary layer at depth  $w$  (see appendix),  $g_w$  is a function giving the fraction of emitted light energy flux, generated by an X-ray quantum absorbed at an elementary thin phosphor layer  $dw$  situated at depth  $w$ ,  $w_0$  is the total coating weight of the phosphor,  $\sigma$  and  $\beta$  are optical parameters related to  $\mu_a$  and  $\mu_s$  as follows:

$$\sigma = [\mu_a (\mu_a + 2\mu_s)]^{1/2}, \quad \beta = [\mu_a / (\mu_a + 2\mu_s)]^{1/2}. \quad (9)$$

$\beta$  has been also expressed [12] as:

$$\beta = \frac{(1 - R_\infty)}{(1 + R_\infty)}, \quad (10)$$

where  $R_\infty$  is the reflectivity of a very thick screen with no light transmission through it,  $\rho$  is related to the reflectivity  $r$  at the phosphor screen–substrate interface by the relation:

$$\rho = \frac{(1 - r)}{(1 + r)}. \quad (11)$$

$\beta$  and  $\rho$  were measured by reflectivity measurements following the technique described by Ludwig [12]. The value of  $\sigma$  as well as the intrinsic conversion efficiency  $\eta_C$  were determined by the fitting, using the Levenberg–Marquard method [13].

## 2 Results and discussion

Figure 1 shows the variation of NEP with X-ray tube voltage for 34 mg/cm<sup>2</sup> phosphor coating weight. NEP initially decreases rapidly with tube voltage and shows a tendency to remain constant at high voltages. The shape of the curves indicates that NEP is mainly dominated by the variation of the quantum detection efficiency ( $\eta_Q$  in formulas (2) and (7)) with X-ray energy. At low voltages, phosphor screens absorb easily larger fractions of the incident X-rays and hence they produce higher quantities of optical quanta than at high voltages. Similar reasoning, based on detection efficiency, may justify the increased NEP values at high coating weights. As it is shown in relation (7), thick screens absorb large fractions of X-rays, which in turn produce high quantities of optical quanta. At high tube voltages, which correspond to higher effective X-ray energies and lower values of  $\mu$  (see relation (7)), NEP should be expected to decrease more rapidly. However, X-ray losses are compensated by an increase in the number of optical photons created within the phosphor mass per X-ray absorbed, given by the ratio  $\eta_C E/E_\lambda$ . While X-ray energy  $E$  increases,  $\eta_C$  and  $E_\lambda$  remain constant. Thus, higher number of optical quanta are finally emitted per X-ray absorbed. The two curves corresponding to front- and back-screen configuration are similar. However, for equal coating weight NEP values are higher in back-screen than in front-screen configuration setup. This may be explained if one considers that, due to the exponential law of X-ray absorption, most X-ray quanta are absorbed not far from the irradiated phosphor surface. Thus, optical quanta directed towards the irradiated surface have to travel shorter distances to escape the screen than quanta transmitted to the non-irradiated back surface. This results in higher values of light transmission efficiency and NEP.

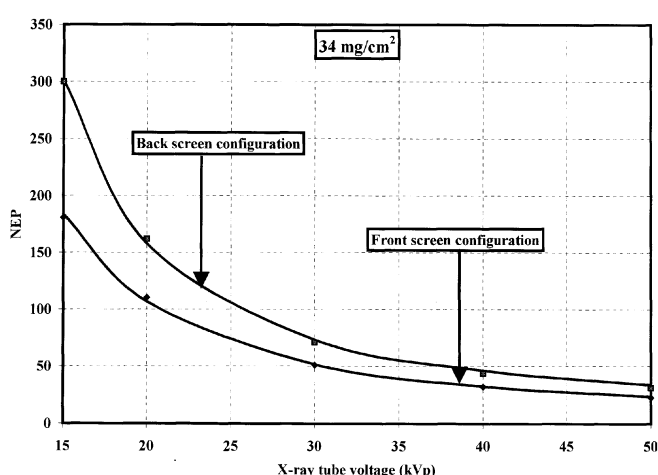


Fig. 1. Variation of the number of optical photons per incident X-ray quantum with X-ray tube voltage for a 34-mg/cm<sup>2</sup> ZnSiO<sub>4</sub>:Mn screen in front- and back-screen configuration setups. Dots: experimental points, solid lines: fitted curves

Solid lines in Fig. 1 represent theoretical curves obtained by fitting (2) to experimental data. Best values of parameters  $\sigma$  and  $\eta_C$  determined by the fitting procedure were  $\sigma = 38 \text{ cm}^2/\text{g}$  and  $\eta_C = 0.08$ . Measured values of  $\beta$  and  $\rho$  were  $\beta = 0.03$  and  $\rho = 0.9$ . The value estimated for  $\eta_C$  is lower than those of terbium-activated rare earth phosphors Gd<sub>2</sub>O<sub>2</sub>S:Tb and La<sub>2</sub>O<sub>2</sub>S:Tb, ranging between 0.13 and 0.2, but it is higher than the  $\eta_C$  value of CaWO<sub>4</sub> (0.04) used in conventional radiographic cassettes [3, 14].  $\sigma$ ,  $\beta$ , and  $\rho$  are similar to those previously found for other green light emitting phosphors Gd<sub>2</sub>O<sub>2</sub>S:Tb, La<sub>2</sub>O<sub>2</sub>S:Tb, ZnSCdS:Ag etc. [9].

Figure 2 shows the variation of NEP with phosphor coating weight for both front-screen and back-screen configurations. The curve representing back-screen data initially increases and exhibits a saturation region for coating weights higher than 90 mg/cm<sup>2</sup>. This curve shape is well suited to the exponential law of X-ray absorption variation with thickness (relation 7). This demonstrates the dominant role of quantum detection efficiency in NEP behavior. The curve corresponding to front-screen configuration shows a tendency to decrease for coating weights higher than 60 mg/cm<sup>2</sup>. This may be explained by considering that in thick phosphor layers the optical quanta directed to the non-irradiated side of the screen have to penetrate longer transmission paths to escape, thus increasing the probability of optical losses.

To compare results obtained for Zn<sub>2</sub>SiO<sub>4</sub>:Mn with another material, similar measurements were performed on Gd<sub>2</sub>O<sub>2</sub>S:Tb. A 90 mg/cm<sup>2</sup> Gd<sub>2</sub>O<sub>2</sub>S:Tb phosphor layer was prepared and tested under the same conditions. Results showed that Gd<sub>2</sub>O<sub>2</sub>S:Tb NEP was slightly lower than that of Zn<sub>2</sub>SiO<sub>4</sub>:Mn at 15 kVp and 20 kVp but it was higher at 30, 40, and 50 kVp.

Figure 3 shows the measured emission spectrum of Zn<sub>2</sub>SiO<sub>4</sub>:Mn together with spectral sensitivity curves of the following optical detectors. 1. The GaAs photocathode, used in third-generation non-medical image intensifiers. 2. The extended sensitivity (ES) 20 photocathode, used in fluoroscopic or digital imaging intensifiers and in photomultipliers of nuclear medicine medical systems. 3. The silicon (Si) photodiode, used in computed tomography X-ray detectors and in CCD arrays of some digital radiography systems. 4. A green-sensitive film used in conventional radiographic cassettes.

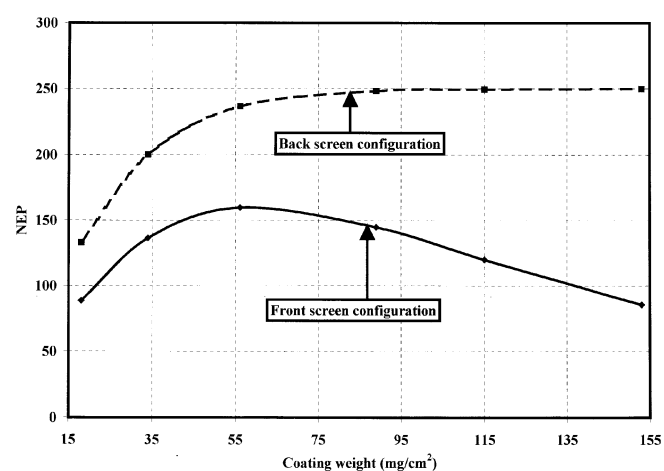


Fig. 2. Variation of the number of emitted optical photons per incident X-ray quantum with phosphor coating weight at 20 kVp X-ray tube voltage

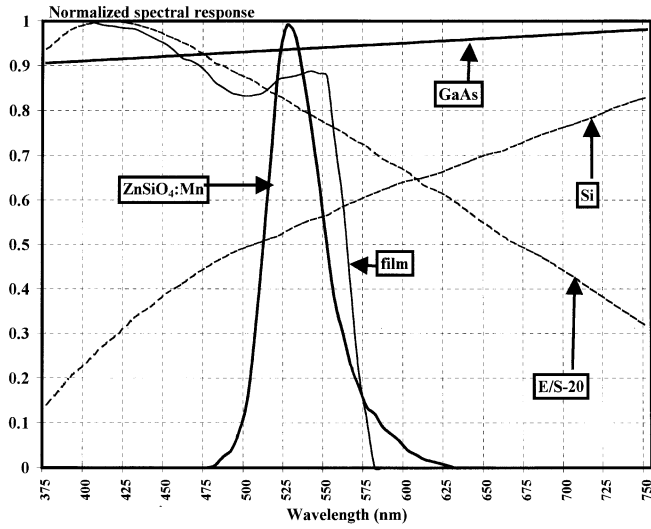


Fig. 3.  $\text{ZnSiO}_4\text{:Mn}$  optical emission spectrum and spectral sensitivity curves of optical detectors

The  $\text{ZnSiO}_4\text{:Mn}$  emission spectrum is centered at 525 nm and it is situated well within the spectral sensitivity limits of the optical detectors. This is very interesting especially for the case of orthochromatic radiographic films, since the latter are designed to detect the spectra of terbium-activated phosphors ( $\text{Gd}_2\text{O}_2\text{S:Tb}$ ,  $\text{La}_2\text{O}_2\text{S:Tb}$ ,  $\text{Y}_2\text{O}_2\text{S:Tb}$ ).

Table 1 shows the values obtained for the matching factor of  $\text{ZnSiO}_4\text{:Mn}$  with the optical detectors as well as matching factors corresponding to  $\text{Gd}_2\text{O}_2\text{S:Tb}$ .  $\text{ZnSiO}_4\text{:Mn}$  is more

Table 1. Spectral Matching factors

Optical Detectors	Phosphors	
	$\text{ZnSiO}_4\text{:Mn}$	$\text{Gd}_2\text{O}_2\text{S:Tb}$
GaAs photocathode	0.938	0.939
E/S-20 photocathode	0.799	0.773
Si photodiode	0.546	0.543
Agfa Curix Ortho GS film	0.775	0.692
Kodak X-omatic GR film	0.742	0.701
Fuji UM-MH film	0.792	0.698

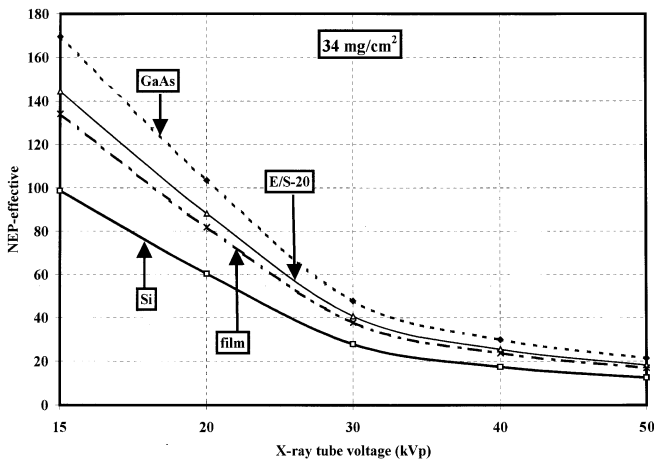


Fig. 4. Variation of effective NEP with X-ray tube voltage, determined in front-screen configuration setup

effective than  $\text{Gd}_2\text{O}_2\text{S:Tb}$  when combined with the three orthochromatic films.  $\text{Zn}_2\text{SiO}_4\text{:Mn}$  is also slightly better when used with the Si photodiode and the ES-20 photocathode.

Figure 4 shows the variation of the effective number of emitted optical quanta per incident X-ray with X-ray tube voltage.  $\text{Zn}_2\text{SiO}_4\text{:Mn}$  shows the highest effective NEP when combined with the GaAs photocathode. However, it must be noted that this photocathode exhibits an almost flat spectral response and is very well matched with all types of phosphor materials. From the rest of the curves of Fig. 4 it is shown that  $\text{Zn}_2\text{SiO}_4\text{:Mn}$  phosphor is better matched with the orthochromatic films and the ES-20 photocathode.

These results show that  $\text{Zn}_2\text{SiO}_4\text{:Mn}$  could be appropriate for use in low-voltage conventional radiography and fluoroscopy, especially in mammographic applications, or in digital imaging systems employing ES-20 photocathodes.

*Acknowledgements.* This study is dedicated to the memory of Prof. G.E. Giakoumakis, leading member of our team, whose work on phosphor materials has inspired us to continue.

## Appendix

### A.1 The function $\Psi_R(E, w)$ :

This function (see relation (8)) is a distribution function that describes the relative probability of an X-ray quantum to interact at an elementary thin layer  $dw$  at depth  $w$  from the irradiated surface [8, 9] of a phosphor layer of coating weight  $w_0$ .  $\Psi_R(E, w)$  may be written as follows:

$$\Psi_R(E, w) = \frac{\mu(E) \exp[-\mu(E)w] dw}{\int_0^{w_0} \mu(E) \exp[-\mu(E)w] dw}, \quad (\text{A.1})$$

where the numerator is the product of  $\exp[-\mu(E)w]$  giving the probability of an X-ray quantum to arrive at depth  $w$ , with  $\mu(E)dw$  giving the probability of X-ray interaction within the thin layer  $dw$ . The denominator is the sum of interaction probabilities within all elementary thin layers of total phosphor coating  $w_0$ . The integral giving  $g_\lambda$  in relation (8), represents the mean value of the light flux fractions  $g_w$  averaged over all thin layers  $dw$ . The values of  $\Psi_R$  serve as weighting factors representing the contributions of the corresponding thin layers, to the light flux emitted by the whole phosphor layer  $w_0$ .

### A.2 The function $g_w(\sigma, \beta, w, \rho)$ :

This function gives the light energy flux produced by the interaction of an X-ray quantum within the layer  $dw$  at  $w$ .  $g_w(\sigma, \beta, \rho, w)$  has been determined as a solution of a diffusion differential equation [15] that describes the propagation of optical quanta through a phosphor material.  $g_w$  has been expressed as:

$$g_w(\sigma, \beta, w, \rho) = \frac{\rho_1 [(\beta + \rho_0)e^{\sigma w} + (\beta - \rho_0)e^{-\sigma w}]}{(\beta + \rho_0)(\beta + \rho_1)e^{\sigma w_0} - (\beta - \rho_0)(\beta - \rho_1)e^{-\sigma w_0}}, \quad (\text{A.2})$$

where  $\sigma$  is an optical parameter called reciprocal diffusion length given [12, 15] by:

$$\sigma = \sqrt{[\mu_a(\mu_a + 2\mu_s)]}, \quad (\text{A.3})$$

$\mu_a$  and  $\mu_s$  being the light absorption and scattering coefficients of the phosphor.  $\rho_0, \rho_1$  are given by:

$$\rho_n = \frac{(1 - r_n)}{(1 + r_n)} \quad n = 0, 1, \quad (\text{A.4})$$

where  $r_0$  and  $r_1$  are the reflectivities at the front-screen interface ( $r_0 \cong 0$  in our case) and at the screen–substrate interface, respectively. Values for  $\rho_1$  and  $\rho_2$  were taken from previous studies [7–9].

$\beta$  is an optical parameter given by

$$\beta = \sqrt{[\mu_a/(\mu_a + 2\mu_s)]}. \quad (\text{A.5})$$

### A.3 The function $\Psi_X(E)$ :

This function describes the incident X-ray energy flux and it may be expressed as

$$\Psi_X(E) = N_X(E)E, \quad (\text{A.6})$$

where  $N_X(E)$  is the X-ray quantum flux (number of incident X-ray quanta per unit of area and time). In the model developed by Tucker et al. [16] for X-ray spectra, the number  $N_X(E)$  of X-ray quanta produced by the bremsstrahlung process with energy between  $E$  and  $E + dE$  is given as follows:

$$N_X(E) dE = [\alpha r_e Z^2 / A] [dE/E] \times \int_E^{E_0} B \frac{(E_e + m_0 c^2)}{E_e} F(E, E_e, E_0) \left[ \frac{1}{\rho} \frac{dE_e}{dx} \right]^{-1} dE_e, \quad (\text{A.7})$$

where  $N_X$  is the X-ray quantum fluence per keV,  $\alpha$  is the fine-structure constant,  $r_e$  is the classical electron radius,  $Z$  is the atomic number of the target material (X-ray tube anode) – usually tungsten or molybdenum.  $A$  is the mass of the target atoms,  $E_0$  is the kinetic energy of the incident electron,  $E_e$  is the penetrating electron energy,  $m_0$  is the rest mass of an electron,  $c$  is the light velocity,  $(1/\rho)[dE_e/dx]$  is the

mass stopping power of the target material,  $F(E, E_e, E_0)$  is the fraction of X-ray quanta transmitted by the anode given by:

$$F(E, E_e, E_0) = \frac{\exp[-\mu(E)(E_0^2 - E_e^2)]}{\rho_A c_{TW} \sin(\theta + \varphi)} \quad (\text{A.8})$$

where  $\mu(E)$  and  $\rho_A$  is the linear attenuation coefficient and density of the anode material, respectively,  $c_{TW}$  is the Thomson–Whiddington constant [16],  $\theta$  is the target angle,  $\varphi$  is the angle off the central axis along which an X-ray quantum travels,  $x$  is the depth of electron penetration within the target,  $B$  is a function of  $Z$  and  $T$  given by Tucker et al. [16].

Most data and functions necessary for  $N_X(E)$  calculations were taken from [16] and from X-ray unit manufacturer's data.

## References

1. Lumilux data book, Riedel-deHaen, Seelze, Germany (1989)
2. R.C. Alig, S. Bloom: J. Electrochem. Soc. **124**, 1136 (1977)
3. B.A. Arnold: *The Physics of Medical Imaging: Recording System, Measurements and Techniques* (American Association of Physicists in Medicine, New York 1979)
4. J.R. Greening: *Fundamentals of Radiation Dosimetry*, in Medical Physics Handbooks (Institute of Physics, London 1985)
5. W.R. Hendee: *Medical Radiation Physics, Year Book* (Medical Publishers, Chicago 1970)
6. G.E. Giakoumakis: Appl. Phys. A **52**, 7 (1991)
7. G. Panayiotakis, D. Cavouras, I. Kandarakis, C. Nomicos: Appl. Phys. A **62**, 483 (1996)
8. D. Cavouras, I. Kandarakis, G.S. Panayiotakis, E.K. Evangelou, C.D. Nomicos: Med. Phys. **23**, 1965 (1996)
9. I. Kandarakis, D. Cavouras, G.S. Panayiotakis, C.D. Nomicos: Phys. Med. Biol. **42**, 1351 (1997)
10. D. Cavouras, I. Kandarakis, A. Bakas, D. Triantis, C. Nomicos, G.S. Panayiotakis: Br. J. Radiology **71**, 766 (1998)
11. E. Storm, H. Israel: *Photon Cross-sections from 0.001 to 100 MeV for Elements 1 through 100, Report LA-3753* (Los Alamos Scientific Laboratory, University of California 1967)
12. G.W. Ludwig: J. Electrochem. Soc. **118**, 1152 (1971)
13. W.H. Press, B.P. Flannery, S.A. Teukolsky, W.T. Vetterling: *Numerical Recipes in C: The Art of Scientific Computing* (Cambridge University Press, Cambridge 1990)
14. P. Haque, J.H. Stanley: Basic Principles of Computed Tomography Detectors, in Radiology of the Skull and Brain: Technical Aspects of Computed Tomography (C.V. Mosby Company, St. Louis, MO 1981)
15. R.K. Swank: Appl. Opt. **12**, 1865 (1973)
16. D.M. Tucker, G.T. Barnes, D.B. Chakraborty: Med. Phys. **18**, 211 (1991)